Chapter 3

Design and development of vehicle test-bed

3.1. Introduction

Electric vehicle technology is currently one of the most researched areas in the world. An electric vehicle has numerous benefits, including a lower carbon footprint and lower noise pollution, making it an almost true green alternative. There have been studies that predict that there will be major transformations in the automobile sector. The Indian government too has launched a Faster Adoption and Manufacturing of (Hybrid and) Electric Vehicles (FAME) scheme under the National Electric Mobility Mission Plan (NEMMP) for 2020 to promote the manufacturing of electric and hybrid vehicle technology [1]. Proper electrification, advanced battery technology, and pollution control in vehicle technology are areas that need constant upgrading, and automakers are working to provide best-in-class facilities in the upcoming vehicles. In highly populated and polluted countries like India, a shift to the electric vehicle domain is much needed, as it will greatly help diminish pollution. The EV industry in India is growing. People are now interested in shifting to electric vehicles. A greener environment will require good EV design so that the carbon footprint and carbon dioxide emissions can be minimised as much as possible. The area of vehicle design is highly intricate due to its multifaceted nature, encompassing various qualities such as spatial considerations, dynamic performance, active and passive safety measures, connection, and more [2]. Advanced battery technologies have renewed interest in battery electric vehicles (BEVs). BEVs are purely electric vehicles that rely on batteries as their energy source for propulsion. Plug-in automobiles, also known as plug-in hybrid vehicles, have emerged as a prominent trend in the development of hybrid automobiles. This is primarily attributed to their capability to enhance the travel range in electric mode and the potential to achieve zero emissions, provided that the distance travelled remains below the charging threshold [3]. Some manufacturers have launched products like the Nissan Leaf and Chevy Bolt EV, which are fully electric. In India, too, companies like Mahindra & Mahindra and Kia

have introduced EV models on the market. The design process involves several aspects, which include both mechanical and electrical components. The mechanical segment includes chassis design, the size of the car, the steering geometry, spaces designated for other components, including energy storage, etc. The electrical part includes the choice of motors, the data acquisition system, and other circuitry involved in the design. The selection of motors and batteries is quite important, as they directly or indirectly affect the energy consumption of electric vehicles.

3.2.Vehicle Dynamics

Vehicle dynamics is the study of vehicle behaviour while it is in motion [4]. It is quite an experimental and analytical technology. In other terms, it describes how the forward motion of a vehicle varies in response to driver inputs, propulsion system outputs, and environmental conditions. It is a crucial component of vehicle design. The vehicle body, suspension components, and tyres are essential system components in vehicle dynamics. Drivetrain and deceleration, suspension and steering, mass distribution, aerodynamics, and tyres are the aspects of a vehicle's design that have the greatest effect on its dynamics [5]**.**

3.2.1. Force and moment

The dynamics of a rigid vehicle can be conceptualised as the motion of a rigid body relative to a constant global coordinate system. The fundamental principles governing the translational and rotational motion of a rigid body are elucidated by the Newtonian and Eulerian laws of motion. The forces acting on a system of interconnected rigid bodies can be classified into internal and external forces within the framework of Newtonian dynamics [5]. External forces are derived from sources that are outside of the system, whereas internal forces arise from interactions between different components within the system. An external force can manifest as either a contact force, such as the traction force exerted on a tyreprint of a driving wheel, or as a body force, shown by the gravitational force acting against the vehicle's body.

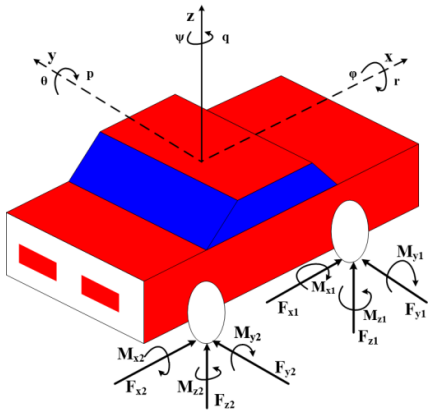

Fig.3.1Forces and moments acting on a vehicle in motion[5]

A force system is defined as the collective influence of external forces and moments exerted on a rigid body, exemplified by the forces and moments acting on the vehicle seen in Figure 3.1. The general mathematical representation of the moment of force exerted on an object is the product of the applied force and the distance between the point of rotation and the line of action of the force, commonly referred to as the moment arm. The concept of moment arm refers to the perpendicular distance between the point at which a force is applied and the axis of rotation.

$$M = F * r_i \tag{1}$$

In this context, the symbol *M* represents the moment of force, while *F* represents the force exerted on the body at a certain location i, denoted by r_i. Torque is described as the moment of a force. The impact of a force system is tantamount to the impact of the resultant force in addition to the moment of the force system. Two force systems can be considered similar if their resulting forces and consequent moments are equal. In the event that the resultant force of a force system is equal to zero, it may be observed that the resultant moment of said force system remains unaffected by the choice of origin within the coordinate frame. The equations of motion in vehicle dynamics are commonly formulated inside a collection of vehicle coordinate frames. The x-axis is a longitudinal axis that traverses through the centre of mass C and is oriented in the forward direction. The y-axis has a horizontal orientation towards the left. The vertical axis, sometimes referred to as the z-axis, is oriented in a perpendicular manner with respect to the ground surface. It is oriented in the opposite direction to the force of gravity,

denoted as g, which represents the acceleration due to gravity. The aggregate or overall force, *F*, represents the aggregate of all external forces exerted on the vehicle by the ground, as depicted in Figure 3.1. This quantity is mathematically defined by equation (2). Similarly, the total moment M is the cumulative sum of all the moments generated by the external forces, as expressed in equation (3).

$$F = F_x\hat{\imath} + F_y\hat{\jmath} + F_z\hat{k} = \sum_k F_k \tag{2}$$

$$M = F_x\hat{\imath} + F_y\hat{\jmath} + F_z\hat{k} = \sum_k M_k \tag{3}$$

Vehicle orientation uses three angles; roll angle ∅ about the x-axis, pitch angle θ about the y-axis, and yaw angle ψ about the z-axis. With reference to the ISO 8855 intermediate system, the roll angle is obtained with a rotation about the forward direction axis of the vehicle. The pitch angle is obtained with a rotation about the lateral direction axis of the vehicle. The yaw angle is measured between the forward direction of the vehicle, projected onto the horizontal plane, and the East[6]. The magnitude of these angles has been denoted by *r*,*p* and *q* respectively and can be expressed in matrices as follows:

$$r = \begin{bmatrix} 1 & 0 & 0 \\ 0 & Cos(\emptyset) & -Sin(\emptyset) \\ 0 & Sin(\emptyset) & Cos(\emptyset) \end{bmatrix} \tag{4}$$

$$p = \begin{bmatrix} Cos(\theta) & 0 & Sin(\theta) \\ 0 & 1 & 0 \\ -Sin(\theta) & 0 & Cos(\theta) \end{bmatrix} \tag{5}$$

$$q = \begin{bmatrix} Cos(\Psi) & -Sin(\Psi) & 0 \\ Sin(\Psi) & Cos(\Psi) & 0 \\ 0 & 0 & 1 \end{bmatrix} \tag{6}$$

3.2.2. Tyre dynamics

Tyres are essential for providing the forces required to operate the vehicle, making them a crucial component of a vehicle. They are the primary component that interacts with the road. Tyre properties have a significant impact on vehicle performance. Tyres have an impact on vehicle traction, riding comfort, and fuel consumption [5]. The tyreprint is the area of contact between a tyre and the road. It is also known as a contact patch or a tyre footprint. The transmission of normal and

friction forces occurs between the road and tyre at any location along the tyreprint. The impact of contact forces can be described by a resultant force system, which encompasses vectors of force and torque exerted at the centre of the tyreprint. It is worth noting that the area of the tyreprint is inversely related to the pressure in the tyre.

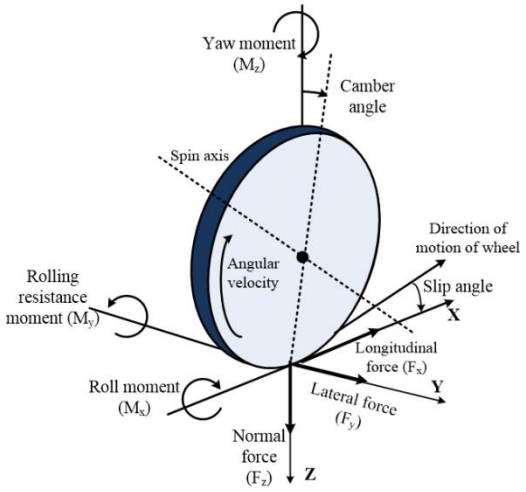

Fig.3. 2 The tyre co-ordinate system[5]

The longitudinal, lateral force as well as vertical systems produced under the tyres during motion help manoeuvre the vehicle. Wheel torque T is the amount of force that the vehicle applies to the tyre as it revolves around the tyre axis. The force system exerted on a tyre by the ground is commonly assumed to be located at the centre of the tyreprint, and can be decomposed into components along the x, y, and z axes. Fig. 3.2 provides an illustration of this. As a result, a 3D force system containing three forces and three moments is created when a tyre interacts with the road. These forces and moments are detailed below [5].

a. Longitudinal force (F_x) - This force is alternatively referred to as the forward force. The force under consideration is exerted in the x-axis direction. The magnitude of this force is positive during vehicle acceleration and negative during deceleration.

b. Normal force (F_z) - This force is alternatively referred to as the vertical force or wheel load. This force is oriented vertically and is perpendicular to the plane of the ground. If

the resultant normal force is directed in an upward direction, it will have a magnitude greater than zero.

c. Lateral force (F_y) - The force in context is perpendicular to the ground and is orthogonal to both the normal force and the longitudinal force. If this force is oriented in the y-direction, it possesses a magnitude that exceeds zero.

d. Roll moment (M_x)- The longitudinal moment about the x-axis is called the roll moment. A positive consequence is observed when there is a tendency for the tyre to rotate about the x-axis. This is also alternatively referred to as the bank or overturning moment, or tilting torque.

e. Pitch moment (My) - The lateral moment around the y-axis is considered positive when it induces a rotational force on the tyre, causing forward movement. This moment is also alternatively known as rolling resistance torque.

f. Yaw moment (Mz) - This moment is directed upward and centred on the z-axis. When the tyre rotates about the z-axis, the resultant is larger than zero. This moment is alternatively called self-aligning moment or bore torque.

3.2.3. Steering dynamics

A steering system is essential for vehicle manoeuvrability. As a result, steering dynamics and vehicle dynamics are tightly intertwined. The essential component of every steering system is the steering wheel or steering handle. Since its conception in 1881, most vehicle manufacturers have used the Ackermann mechanism for steering devices [5]. Though systems have evolved, the fundamentals of all systems remain the same. A shaft translates steering input into wheel motion using a steering system that incorporates gear reductionRack-and-pinion or recirculating ball bearings are frequently employed for the purpose of achieving reduction.

According to research, rack-and-pinion steering is widely employed as the predominant steering mechanism in passenger vehicles [5]. The positioning of the rack can be found either in front of or behind the steering axle. The transmission of the steering force to the steering linkage occurs through a mechanical component referred to as the Pitman arm. In order to achieve optimal manoeuvrability, it is necessary for passenger vehicles to possess a minimum steering angle of around 35 degrees at the front wheels. The calculation of the steering ratio involves the division of the rotation angle of the steering wheel by the steering angle of the front wheels. The majority of street automobiles typically possess a steering ratio of approximately 10:1. According to the literature, it has been observed that Ackerman steering systems consist of distinct steering ratios for both the inner and outer wheels [5]. Additionally, it demonstrates non-linear characteristics and is influenced by the angle of the wheel.

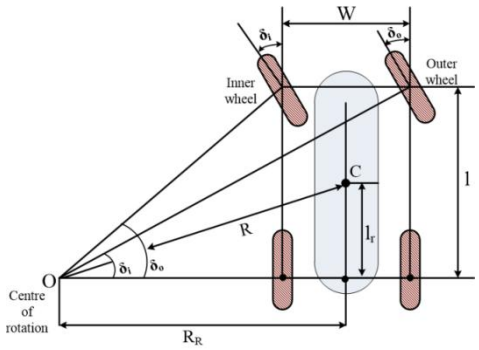

Fig.3.3 A front-wheel-steering vehicle and steer angles of the inner and outer wheels.

The trackwidth, denoted as *W*, refers to the measurement of the distance between the steer axis of the steerable wheels. The wheelbase refers to the distance between the front and rear axles. The parameters *W* and *l* are also commonly referred to as the kinematic breadth and length of a vehicle, respectively. The mass centre of a vehicle in motion will revolve around a circle of radius *R*.

$$R = \sqrt{l_r^2 + l^2 cot^2 \delta} \tag{7}$$

and

$$\cot \delta = \frac{\cot \delta_o + cot\, \delta_i}{2} \tag{8}$$

The cot-average of the inner and outer steer angles has been denoted by δ. For the wheels to rotate without constraint on a curved road, it is necessary for the normal line to the centre of each tyre-plane to intersect at a shared point. Figure 3.3 depicts

a vehicle with front wheel steering executing a left turn which adheres to the principles of Ackermann steering geometry. Consequently, the turning centre O is situated on the left side, with the inside wheels being the nearest left wheels to the centre of rotation. Ackermann geometry is a mechanism that enables steering in accordance with the Ackermann condition. It is necessary in situations where the vehicle's velocity is insufficient and the slip angles exhibit negative values. The lateral and centrifugal forces do not reach a state of equilibrium. The Ackermann steering condition, alternatively referred to as the kinematic steering condition, is characterised by its zero-velocity and static nature.

3.3. Selection of vehicle prototype

Eco-routing systems in electric vehicles are linked to the area of navigation in transportation. It includes the estimation of energy consumption as well as the driving range of an EV during a particular trip. The estimation process involves the acquisition of various parameters in real time. A dynamic test bed is required for obtaining the parameters in real-time on board the vehicle during a trip. This work is purely research based and the main motive is to estimate range and energy to demonstrate an eco-route. The proposed design consists of a system for estimating the energy consumption of electric vehicles. The EV prototype has therefore been designed and developed indigenously in the laboratory. The EV has been developed to match our requirements for estimating energy consumption during a trip. The choice of vehicle made is a neighbourhood electric vehicle (NEV). A NEV is mainly used for short trips around the campus or community. It has also been reported that cities are currently developing roads for NEVs in an effort to reduce vehicle emissions, reduce roadway deterioration, and reduce reliance on fossil fuels [7]. A NEV model has been selected because it is best suited for our research purposes. Since our work mainly emphasises the techniques and not the vehicle type, it is an optimal choice. It is purely electric and lightweight. The EV has been designed to carry a single passenger since that is the minimum requirement for demonstration of an eco-routing system. Different sensors have been attached to the EV for the extrapolation of parameters that contribute to the measurement of energy consumption. Road tests performed on the EV allow data acquisition, which is then used for energy estimation using the road

load model. The eco-routing, or energy-efficient route, has been demonstrated with the help of results attained from the on-road tests.

3.3.1. Mechanical design

A test vehicle is a necessary component of the research work because various elements of eco-routing, like energy consumption and range, can only be analysed under on-road conditions. The development and design of a test electric vehicle prototype has been completed as a part of this research work. The dynamic testbed that has been built is a light-weight neighbourhood battery electric vehicle (BEV) and is independent rear-wheel-driven. The EV has a curb weight of approximately 120 kg, a track width of 103cm, a wheelbase of 145 cm, and a wheel diameter of 42cm. The chassis is purely made of iron rods. It is to be highlighted here that the entire vehicle prototype has been constructed in the research laboratory from chassis level itself. It has been solely designed and built for the purpose of this research work. All experiments related to this research work have been performed only on this electric vehicle prototype. A few illustrations of the test EV at different stages of its development are provided as follows. Fig. 3.4 and Fig.3 5 show the top view and the front view of the test EV chassis, respectively. The white strings in the figures have been drawn to maintain the Ackermann ratio so that the EV does not slip while taking turns. The front suspension has been shown in Fig. 3.6. This test vehicle uses two separate 24-volt, 350-watt permanent magnet DC motors (PMDC) placed at the rear end of the vehicle. The whole set-up of motors attached to the swing arm is depicted in Fig. 3.7. These motors are used to drive the rear wheels of the EV, which in turn propel the vehicle forward. The transmission system in the EV uses a two-tier belt drive. The motors are connected to the wheels through a pulley using belts in a gear ratio of 1:5. The gear ratio has been adjusted to maintain a maximum speed of 16km/hr for the test vehicle. The EV uses dedicated drive circuits, which help run the motors. A 24V power supply is applied to run both the motors, which are acquired from a 24V 40Ah Lithium-ion (Li-ion) battery. The battery unit is placed on the front left side of the vehicle. A main switch has been connected just after the battery in series for better control of the entyre drive system. The system also has an accelerator and a mechanical brake pedal. An electrical brake system is also connected to the mechanical brake

to ensure that the braking system is foolproof. The vehicle is a single-passenger vehicle. The swing arm supports the main vehicle body and holds the shock absorber in place. The shock absorber assists the lower swing arm, which is responsible for load bearing, and in our test EV, it also holds the propulsion motors. The test EV has been successfully developed, and test runs have been performed to obtain information on load and road conditions, which in turn helps in the energy consumption estimation of the vehicle. The final look of the test vehicle is illustrated in Fig. 3.8. The dimensional features of the EV have been tabulated below in Table 3.1.

Table 3.1 Features of the EV prototype (dynamic test bed)

Kerb weight	~120kg
Wheel base	145 cm
Track width	103 cm
Wheel Diameter	42 cm
Battery	24 V/40Ah Li-ion
Motors	350 W PMDC motor

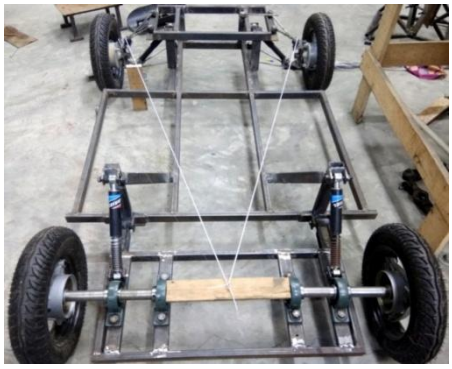

Fig.3.4 Top-view of the chassis of the test EV prototype

Fig.3.5 Front-view of the chassis of the test EV prototype

Fig.3.6 View of the front suspension

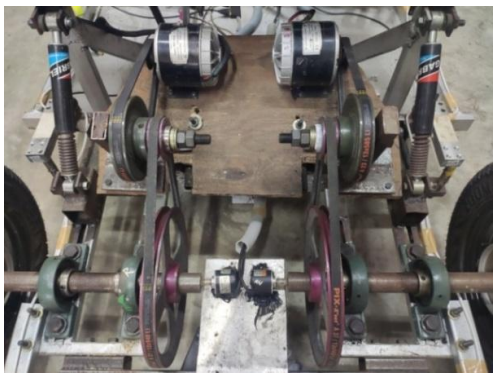

Fig.3.7 Connection of the motors to the wheels for power transmission

Fig.3.8 The test EV prototype after its completion

It has already been mentioned that the test electric vehicle prototype has a belt-driven transmission system. The belt drive is a power transmission drive system that transfers power from one rotating shaft to another using a belt. The belt drive is adaptable and widely used in equipment such as machines and vehicles that require smooth and silent operation [8]. The belt-drive power transmission system consists of two or more pulleys connected by a tensioned belt. The pulley that receives power is known as the driven pulley, while the pulley that transfers power is known as the driver pulley. It is made up of two parallel shafts, a pulley positioned on the shafts, and a belt that runs across the surface of the pulley. This method of installation is inexpensive. The noise level is lower when compared to chain drives. Belt drives also require extremely little upkeep. They are far more resistant to environmental pollution than chains and do not rust. High-quality belts often have an efficiency of 95 to 98%, making them an efficient option [9].

3.3.2. Electric Drive and circuitry

The electric drive of the dynamic test bed consists of a DC motor controller and a data acquisition system. The motor controller system can be said to be the heart of the electric vehicle. The Intelligent Motor Controller (IMC) employs a microprocessor for the regulation and management of electrical components utilised in motor control applications. A controller is often designed to facilitate the

initiation, cessation, regulation of velocity, reversal, and protection of a motor. The test EV consists of two separate motor controllers for each of the two PMDC motors. Each controller has an aluminium body and has dedicated terminals for connecting the power source, the motor, the input source, a power switch for protection, and also, brakes. The block diagram of the motor controller unit as well as the circuitry used in the test vehicle prototype have been depicted in Fig.3.9 and Fig.3.10 respectively. The controllers connect the battery to the motors, which are in turn used for vehicle propulsion. The controller unit encompasses the gate drive, switching, and snubber unit within it. The switching unit consists of three power MOSFETs connected in parallel to handle large amounts of current and reduce conduction losses. The armature voltage of the motors is controlled using a pulse width modulation technique, which in turn controls the speed of the motors. The technical specifications for the motor control unit are tabulated in Table 3.2.

Table 3. 2 Technical specifications of motor controller

Rated power	350 Watts
Current limit	21Amperes
Rated voltage	24 Volt DC
Under-voltage protection	20V
Dimension of controller unit	73mm X 58mm X 36mm(L X W X H)

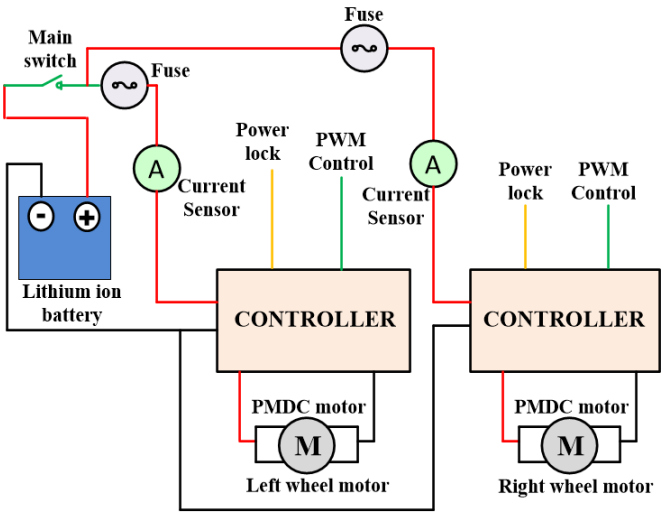

Fig.3.9 Block diagram of the motor contol circuit

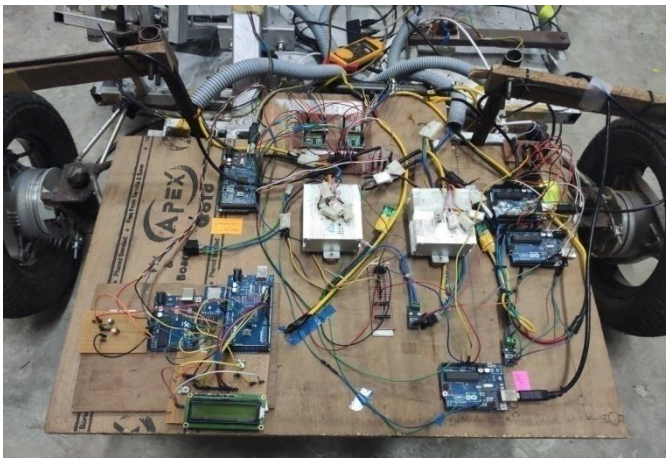

Fig.3.10 Circuitry involved in the test EV

3.3.3. Sensor interfacing and data acquisition

The dynamic testbed is equipped with a number of sensors that help determine the parameters necessary to calculate its energy consumption. Data from these sensors will eventually aid in determining an eco-route or calculating the route with the lowest energy consumption. The vehicle utilises microcontroller circuits for both control and data acquisition. Four load sensors were used to compute the force on the wheels; two accelerometers were used to measure the road grade or tilt angle; and two encoders were used to measure the test EV's speed and acceleration. Connected sensors are digital sensors from which data can be readily collected for further calculations. Since on-road testing of the test electric vehicle necessitates real-time data for energy consumption estimation, all data from these sensors is collected in real-time. All the collected information has been stored on a computer. This information has been further processed to estimate various parameters necessary for estimating the energy consumption of a vehicle during a specific voyage. The sensors that have been fitted to the test EV for data acquisition are described in the following section:

i. Load sensor

A load cell is a transducer that converts forces like tension and compression into an electrical output that can be measured [10]. There are numerous types of force sensors, but strain gauge load cells are the most prevalent. Load cells are considered more precise transducers than other apparatus or instruments.

Load cells are strongly recommended for any force measurement application. Strain sensors are attached to a spring material to construct a load cell. Strain sensors are bonded to the area of the spring material where the strain will be greatest in order to detect it accurately. Strain gauges transmute the strains generated in the spring material upon application of an external force into a change in spring resistance. A load cell is based on an electrical circuit called the Wheatstone Bridge. Since the resistance change is very small, a wheatstone bridge, a circuit used to detect small resistance changes, is employed. Wheatstone bridge is the four-resistor network as depicted in Fig. 3.11. The fundamental basis of a load cell's operation is rooted in the observation that the electrical resistance of a conductor undergoes alteration when subjected to strain-induced variations in its length [11]. When connected to an appropriate measuring circuit, the strain gauge's change in resistance can be used to measure strain with high precision.

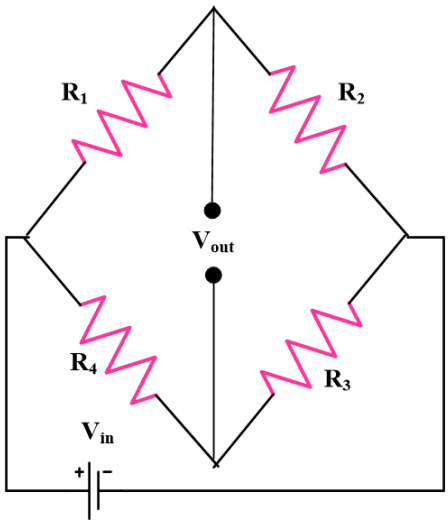

Fig.3.11 Wheatstone Bridge Configuration of a load cell

Four load cells with an individual capacity of 200kg are attached to each of the four wheels of the test EV. The straight-bar load cells made of aluminium are able to convert up to 200 kg of force into an electrical signal. The electrical resistance that varies in reaction to and proportional to the strain imparted to the bar can be measured by each load cell. The HX711 analog-to-digital converter is linked to each cell's four lead wires. This sensor is used to amplify and digitalise the load cell output to which it is directly interfaced. The driving voltage, which ranges from 5 to 12 volts, generates the output voltage in

response to changes in applied force. Four strain gauges connected in a Wheatstone bridge configuration make up these load cells. When the vehicle is moving, the force at the wheels changes constantly, changing the information about the load. The load cells can be used to effectively record this. After processing the data, weight and load values can be determined.

ii. Encoder

An encoder is a device used in position sensing that can recognise mechanical motion and transform it into an output signal with an analogue or digital code. Position is a parameter that is directly measured, but velocity, acceleration, and direction can be determined by deriving them from the position, whether it is in a linear or rotating motion [12]. The angular location of a rotating shaft can be obtained by utilising it. The electrical signal generated by the rotating movement can be classified as either analogue or digital, depending on its characteristics. To record the vehicle's speed information, two rotary encoders have been attached to the axles of the rear wheels. 600 PPR Incremental Optical Rotary Encoders have been used as encoders. They have quadrature outputs for increment counting and are high-resolution optical encoders. It provides 2400 transitions between outputs A and B each spinA quadrature decoder is required in order to convert the pulses into an ascending count. The rotation of wheels in the test EV causes the shaft of the rotary encoders to turn as well. The pulses are counted, and the information about the pulse rate can be used to determine the vehicle's speed. The rotary encoder's technical specifications are provided in the table below. Fig. 3.12 (a) shows the pictorial representation of an incremental rotary encoder. Fig 3.12 (b) illustrates the circuit diagram of the encoder. The encoder contains four wires which comprise the supply (red), ground (black), phase A output signal (green), and phase B output signal (yellow). A 5V input voltage has been supplied to the encoder. To mitigate interference in the output and get accurate logical output values from the encoder, two pull-up resistors with a resistance of 1.5 kilohms each were incorporated into both the A and B phases of the encoder output. Additionally, this circuitry serves to safeguard the open collector output-triode

against potential harm resulting from a direct short circuit in the Vcc supply. Table 3.3 lists the technification of a rotary encoder.

Table 3. 3 Technical specifications of rotary encoder [12]

Encoder type	Incremental
Operating voltage	5 – 24 Volts
Current consumption	≤ 40 mA
Maximum speed	5000 rpm
Pulse per revolution	600 ppr
Counts per revolution	2400 cpr

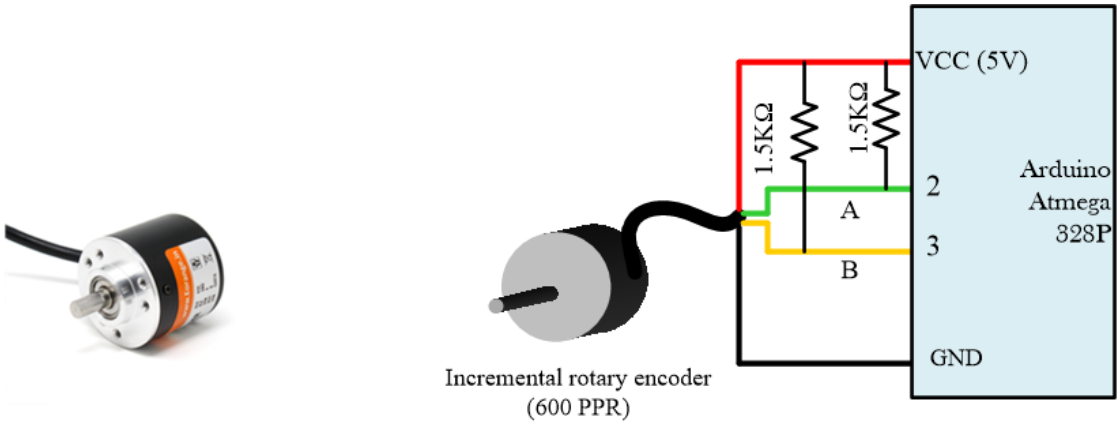

Fig.3.12(a) Illustration of an incremental rotary encoder [12] and (b) Circuit diagram of the encoder

iii. Hall effect current sensor

A Hall Effect current sensor module is one of the most user-friendly and accurate sensors for determining AC or DC current. It detects the presence and magnitude of a magnetic field using the Hall effect [13]. The ACS712 integrated chip is utilised in the module to sense current. The sensor module is shown in Fig. 3.13. The Hall effect integrated circuit (IC) converts the magnetic field generated by the current passing through the copper conductor into a corresponding voltage. The proximity of the magnetic signal to the Hall transducer enhances the precision of the device. The BiCMOS Hall IC, which

is chopper-stabilized and has a low-offset, is programmed for accuracy post-packaging [14]. This IC provides a highly accurate and proportional voltage output. Due to an incorporated hall sensor, the sensor can even monitor high AC mains current while remaining separated from the measuring component. The 5V current sensor generates an analogue voltage that is proportionate to the current that is sensed on the sensing terminals. Microcontrollers can be used to read the values.

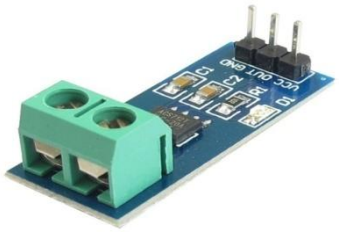

Fig.3.13 A Hall-effect Current Sensor Module[15]

The test EV is equipped with two separate current sensors for recording the current consumption of both the motors. The data from the output terminal of the sensors are read into the PC interfacing with Arduino. The total current consumption of the vehicle can then be summed up. The details of the sensor are tabulated below in Table 3.4.

Table 3.4 Technical specifications of hall effect current sensor[14]

Sensor IC	ACS712
Supply Voltage	5 V
Internal Conductor resistance	1.2 mΩ
Measurement Current range	± 30 A
Sensitivity	66 V/A

iv. Accelerometer

An accelerometer is a device that detects the acceleration of a moving body or its vibration. The piezoelectric material squeezes under the force of vibration or a change in motion, producing an electrical charge proportional to the force applied. The piezoelectric material undergoes compression in response to vibrational forces or alterations in motion, resulting in the generation of an electric charge that is directly proportionate to the applied force. Given that

force is directly proportional to charge and mass remains constant, it follows that acceleration is also directly proportional to charge. Accelerometers are sensitive to both linear acceleration and the gravitational field in their immediate vicinity [16]. The test EV employs the MPU 6050 sensor module to estimate the vehicle's tilt angle or pitch. The data is then processed to acquire information regarding the road grade present in each patch at any given time. Four separate accelerometers have been affixed to the four wheels of the EV. The MPU-6050 is an accelerometer and gyrosensor instrument with three axes. It contains a variety of features. It offers programmable digital output with full scale ranges of 2g, 4g, 8g, and 16g [17]. The utilisation of integrated 16-bit analog-to-digital converters (ADCs) enables the concurrent sampling of accelerometers, eliminating the requirement for an external multiplexer. Normal operating current is approximately 500μA.It has an 8 kHz sampling rate. This sensor is compatible with the I2C interface protocol. The vibration sensitivity is also high, resulting in rapid device communication.

All the sensors have been calibrated and checked individually before the test run of the electric vehicle prototype. The sensors are simple and easy to use. Moreover, the results obtained from them are all in real time, which is then used for the calculation of energy consumption during a trip as well as the demonstration of an eco-route. Fig. 3.14 shows a pictorial representation of the placement of sensors in the prototype vehicle.

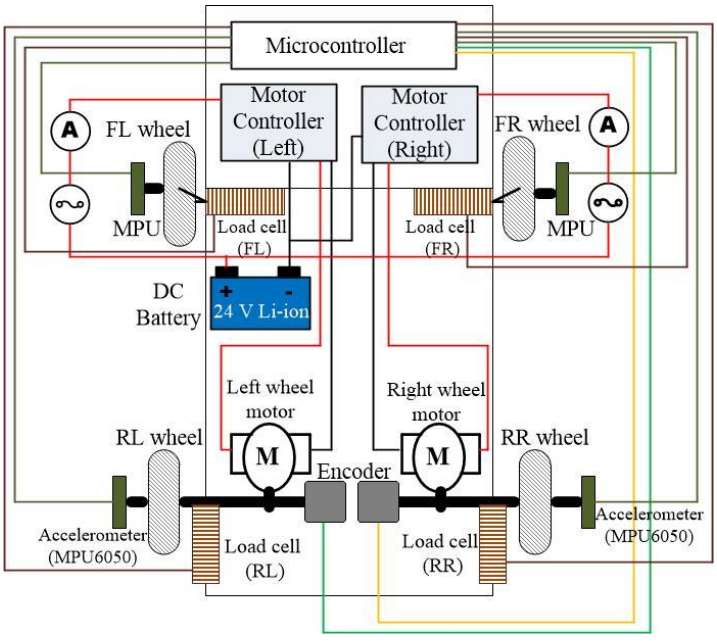

Fig.3.14 Placement of sensors in the vehicle

Data acquisition is an important aspect of vehicle design and development. It is a process that entails sampling signals used to measure actual physical occurrences in order to digitally transform them so that a computer and software can alter them [18]. A system that consists of measurement tools, sensors, a computer, and data collection software is known as a data acquisition system. Data is collected, stored, processed, and visualised using a data capture system. This entails gathering the data necessary to comprehend electrical or physical processes. Sensors, signal conditioning, analog-to-digital converters (ADC), and a laptop or computer for data logging and recording are the essential elements of a data acquisition system. The test EV has sensors installed, which are linked by microcontroller boards. The laptop, which is connected to the microcontrollers, creates a conduit for data recording and storage. The EV uses two different types of microcontrollers. They are the Atmega2560 microcontroller chip found in the Arduino Mega board and the Atmega328P microcontroller chip found in the Arduino UNO microcontroller board. The microcontroller boards are attached to the laptop through serial ports and contain an integrated ADC capability. Fig. 3.15 shows how all of the sensors are connected to the microcontroller boards. The connections are all displayed in depth. Through these boards, all sensor data has been captured in real time and logged into a laptop for subsequent analysis.

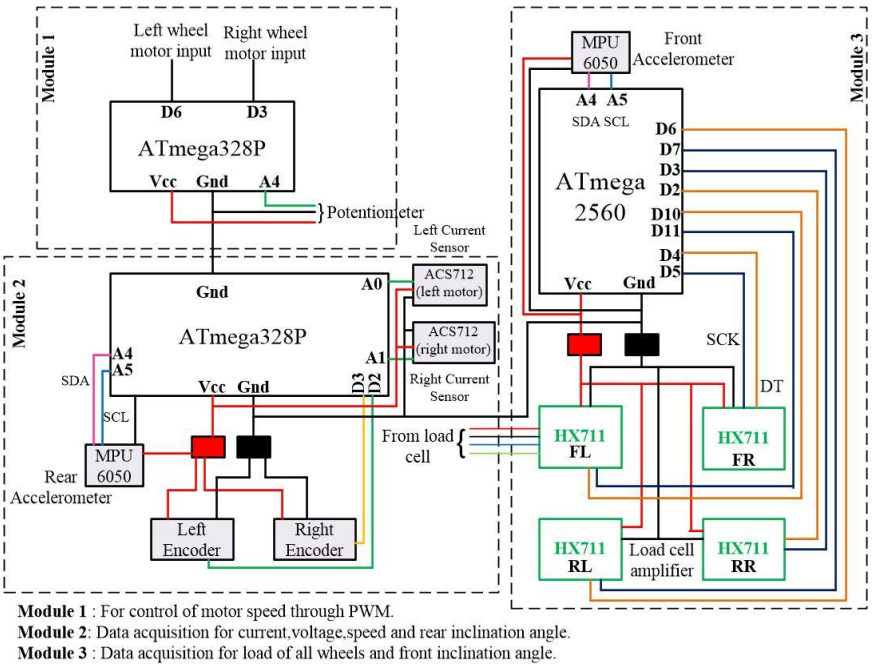

Fig.3.15 Connection of sensors to the respective microcontrollers for data acquisition

3.4.Parameter extraction of Direct Current (DC) motors

The increasing popularity of electric vehicles (EVs) necessitates the use of energy-efficient, dependable, and cost-effective electric propulsion motors. However, the search for the ideal motor becomes quite complicated when vehicle dynamics and the design of electric vehicles are considered. Motors are deemed most efficient when their efficacy is typically around 75% of their rated load. It has been discovered that a motor's efficiency drastically decreases at approximately 50% capacity [19]. During manoeuvres, the driving motor of an EV experiences inconsistent variations in load due to factors such as road grade and road condition, which influence a vehicle's energy consumption [20]. It is essential that the motors are operated at maximum efficacy, thereby contributing to the vehicle's overall energy conservation. This is facilitated by the torque speed characteristics of a drive motor, which also afford the opportunity to manipulate the precise loading conditions on the road. It also provides the circuit designer with the necessary information to drive the motor consistently at the intended efficiency. With these characteristics, one can ascertain the relationship between torque, speed, power, load, etc.

A study of the relevant literature reveals the design and development of various methodologies for characterising various motor types. Diverse techniques for parameter estimation of direct current (DC) motors have been extensively presented [21-22].Researchers have also used neural networks, genetic algorithms, gradient methods, and particle swarm optimisation algorithms to extract the parameters of various motors [23–24]. However, motor parameter extraction methods that are much more general and universally applicable have received little attention. In conventional procedures, a mechanical load is utilised, which necessitates complex designs and increased user effort for the application of larger loads. Such masses are typically pulled by pulleys and belts and experience an unaccounted-for frictional loss. In addition, they require additional measuring instruments, such as a spring balance or torque metre. Also, most of those systems are manual and require the involvement of more than one person. Therefore, in this section, we have presented two automated techniques for the extraction of DC motor parameters in real-time. The first has been done with the help of a mechanical load. The system is simple and easy to use. The second technique uses the application of an electronic load instead of mechanical, so mechanical help has been reduced to a large extent. Electrical loads have promising

advantages over mechanical loads. Because there is no loss due to friction, the accuracy of these loads is higher than their mechanical counterparts. It also minimises the system's overall weight and flexibility. Electrical loads can be changed in a large range, whereas mechanical loads are limited by the setup. Attempts have been made to make the configuration as easy and efficient as feasible. Both the test setups have been created with commercially available electronic components and interfacing tools that are both cost effective and user friendly.The system outputs are obtained in real time, so they can be used on board electric car test systems without any difficulty.

3.4.1. Importance of Torque-speed characteristics

Motor parameter characterization is required for electric motor-based applications. The extraction of torque-speed parameters requires complex and costly instrumentation. Such estimation is critical in research areas such as automobile technology and power generation. An easy method for evaluating these factors without the need for complex systems might be highly beneficial, especially in the case of electric vehicle design. Torque speed characteristics are an essential component of every motor and drive analysis. It is also used in the drive systems of electric vehicles. According to Dr. Huge D. Young, torque can be described as a numerical representation of the ability of a force to induce rotational movement or alter an existing rotational motion. The moment of a force [25] is responsible for generating or altering the rotational motion. In the case of an EV, the motors utilised for traction face uneven load changes due to a variety of factors, such as road gradient and undulations. The capacity to view and record load information in real time would thus be extremely useful to EV designers. It also supplies important information to the drive-circuit designer, who is concerned with vehicle stability and efficiency.

a. DC Shunt motor

The shunt-wound DC motor is categorised as a self-excited DC motor due to the fact that the field windings are linked in parallel with the armature winding [26]. The armature and field windings experience the same supply voltage as a result of their parallel connection. As depicted in Figure 3.16, the schematic of a DC

shunt motor illustrates the separate paths through which the armature current and field current traverse. In this context, V represents the applied voltage, while E_b denotes the reverse emf induced as a result of the rotation of the armature in a DC motor, which is driven by a torque. The counter emf exhibits a direction that is contrary to that of the externally supplied voltage. The variables R_a and I_a are used to denote the armature resistance and armature current, respectively.

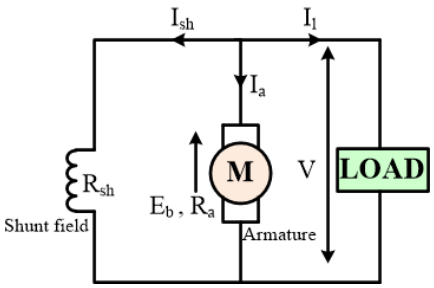

Fig.3.16 Circuit diagram of DC Shunt motor

The DC motor voltage equation is given by

$$V = E_b + I_a R_a \tag{9}$$

The expression for back e.m.f. can be written as

$$E_b = \frac{P\phi ZN}{60A} \tag{10}$$

Where, P is the number of poles, ϕ represents flux per pole, Z is the armature conductor number, N denotes speed of the motor and A is the number of parallel plates. The armature torque for a specific machine can be expressed as

$$T_a \propto \phi I_a \tag{11}$$

In case of shunt motors, flux per pole is constant and so the torque is generally directly proportional to the current in the armature. The speed of a DC motor can be obtained from the equation

$$N = K\frac{E_b}{\phi} \qquad \text{Where, } K = \frac{60\,A}{PZ} \tag{12}$$

Therefore, from the aforementioned equations it can be clearly stated that speed and torque is directly proportional in case of DC motors. The figure , Fig. 3.17 illustrates the speed torque characteristics of the shunt motor.

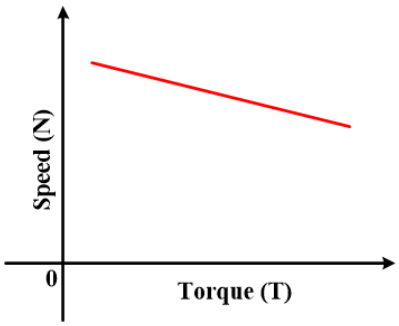

Fig.3.17 Torque-Speed curve of DC shunt motor

b. Permanent magnet DC motor

Permanent Magnet DC (PMDC) motors are a type of direct current (DC) motor that employ poles constructed from permanent magnets. The structure of these motors closely resembles that of a conventional DC shunt motor, with the exception that the stator winding is replaced by permanent magnets to generate the magnetic field. The magnets with radial magnetization are strategically placed along the inner circumference of the cylindrical body of the stator [27]. The magnetic flux is directed back through the stator of the motor to complete its circuit. The rotor of the system is equipped with a direct current (DC) armature, which consists of brushes and commutator segments. Figure 3.18 depicts a concise schematic representation of a PMDC motor.

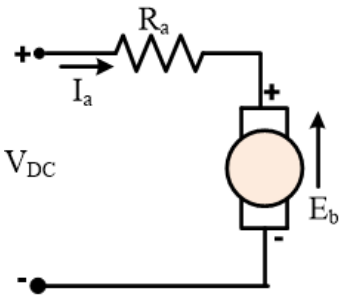

Fig.3.18 Circuit diagram for PMDC motor

Fig. 3.19 depicts the optimal relationship between torque and speed of a PMDC motor. Torque-speed parameters are important properties for electric motors for designing drives [27]. Torque (T) in PMDC motors as written in equation (13) is

$$T = 2nrBIl \tag{13}$$

Where r is the radius of the coil and n denotes the armature turns. The term 2Blr can be replaced by Φ, aggregating the total flux passing across the coil.

$$T = K_t \Phi I \tag{14}$$

The motor torque constant, denoted as K_t, is influenced by various factors, including the number of turns in each coil, the number of pole pairs, and other pertinent characteristics of motor design. Equation (14) clearly depicts that the motor torque is directly proportional to the armature current I. The armature current supply is dependent on the voltage supplied to the motor, E_s and the armature resistance R_a. The rotation of the motor allows the armature to move in a magnetic field. The voltage generated can thus be expressed as

$$K_b = Blv = 2nBlr\omega \tag{15}$$

This voltage is called the back emf and K_b is known as the back emf constant. The constant 2 in equation (15) is because the armature has two sides, where r is the radius and ω is the angular velocity and n is the number of turns. The relation between K_b and K_t can be written as :

$$K_b = K_t \emptyset \omega \tag{16}$$

This voltage acts in opposition to the supplied voltage E_s, resulting in a decrease in the current flowing through the motor. Consequently, the net voltage across the armature can be determined by subtracting the back electromotive force (EMF) from the supply voltage. The armature current is therefore obtained as:

$$I = \frac{V}{R_a} = \frac{K_b - E_s}{R_a} \tag{17}$$

The final relation between torque and rotational speed can so be derived as

$$T = \frac{K_t \emptyset E_s}{R_a} - \frac{(K_t \emptyset)^2}{R_a} \omega \tag{18}$$

Here, E_s refers to supply voltage, R_a is the armature resistance of the motor and ω is the angular speed. Equation (18) illustrates that the torque exerted by this type

of motor maximises at zero velocity, during a state of stalling, and afterwards diminishes progressively as the speed increases.

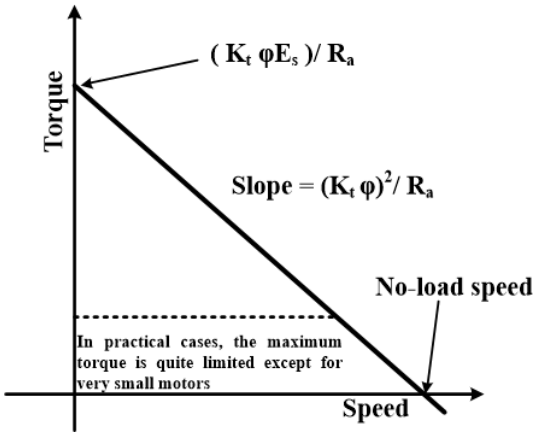

Fig.3.19 Torque-speed characteristics of a PMDC motor (Source: [9], p.145)

3.4.2. Extraction of motor parameters with mechanical load

This section represents an attempt to develop and implement an automated system that analyses motor properties in a real-time drive application. Various key properties of any motor, such as speed, torque, and efficiency, can be extracted very effectively in real time with this technique. Sensors, signal conditioning systems, data collection systems, and the motor control unit make up the entyre system. The block diagram of the system is shown in Fig. 3.20. The system has been tested and validated using two distinct types of DC motors: a Permanent Magnet Direct Current (PMDC) motor and a Shunt DC motor. The validation results lead to the conclusion that the constructed system is viable, and the obtained results closely match the analytical calculations.

A proper mechanical framework is necessary for the attachment of the motor and the other sensors for data extraction in order to determine the torque speed characteristics and efficiency of any motor. The design should also be suited for testing many types of motors, such as induction and AC motors. Testing a motor on a test bench for performance parameter evaluation can provide critical information regarding a motor's appropriateness for a certain application. The system is divided into two parts. The first is a PWM-controlled DC-DC converter for controlling the motor's speed by adjusting the armature voltage. The data acquisition system, on the other hand, reads the voltage across the armature terminal, the current running through the motor, the motor RPM,

and the torque exerted by the motor. A belt and pulley combination has been used for the mechanical framework. One end of the belt is attached to a load cell, while the other, which is looped around the pulley, is attached to a bolt. Tightening the bolt facilitates the determination of torque in this process.

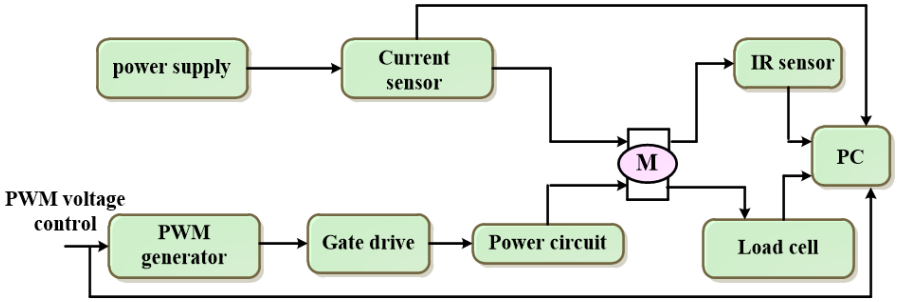

Fig.3.20 Block diagram of the designed system

The shaft of the motor being tested has a small generator attached to it that spins at the same speed as the motor being tested. Calibration techniques have been used to determine the motor's speed. A 1 Horsepower (hp) Permanent Magnet Direct Current (PMDC) motor has been used to test the system. The motor speed is adjusted using a pulse width modulation (PWM) armature voltage control method. The inputs from load cell were gathered and amplified in order to calculate the torque. High-frequency noise components are present in the load cell's output, but these have been reduced by utilising a second-order low-pass Butterworth filter with a very low cutoff frequency. Different loads have been applied to the clamped motor to calibrate the load cell.

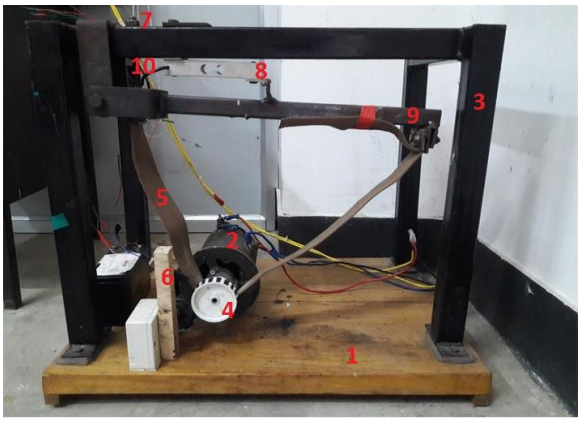

Fig.3.21 Mechanical design of the set-up.

The mechanical set up of the system is as shown in Fig.21 . The major parts of the test bench include Wooden Base (1), Motor Mounting (2), Metal Housing

(3), Pulley attached to the shaft of the motor (4), Belt (5), IR Sensor (6) Tightening Bolt (7), Load Cell (8), Arm (9) and Output of the load cell (10). The numbers in the brackets refer to the numbers in the figure shown above.

3.4.2.1. System design

The torque that the motor exerts and the angle at which the shaft is turning must be determined in order to ascertain the characteristics and efficiency of the motor. The output power of the motor at that precise moment is calculated as the product of the torque produced and the angular velocity. Using a belt and pulley configuration, the motor's torque has been calculated. The force exerted on the load cell is increased by the belt's connection at one end to an arm. The belt's connection to the arm is placed in order to exert the most force. The other end of the belt is then secured to a bolt after being wound around the pulley. When the bolt is tightened, the belt's length decreases, increasing the friction force on the pulley. The pulley generates a clockwise torque as the friction between the belt and the pulley rises. The load cell generates torque in the opposite direction of this torque to balance it. Due to the fact that the system is in equilibrium and the two torques are equal, the force acting on the load cell may be calibrated to determine the torque of the motor being tested. All types of motors can be tested with this method because it is versatile. However, since the vehicle prototype that has been constructed will use PMDC motors for propulsion, the experiments have been restricted to DC motors. The mechanical section incorporates various loading provisions for the motor. In addition, motors bigger than the rated load cell capacity can also be tested using it. This can be done by extending the arm in the fixed-position position, where one end of the belt is. The system is built using a mathematical model to extract torque results even for small quantities. The geometry of the section to determine the position of maximum torque is depicted in Fig. 3.22. The coefficient of friction is taken into account in the calculations for locating the maximum torque. The flat pulley is made of cast iron. It is necessary to choose the belt's material carefully in order to maximise frictional force. The lengthening of the arm, x, increases the force acting on the load cell. By decreasing the angle φ ,caused by an increase in arm length, the perpendicular component of the force, Fsin φ ,

also reduces. As a result, the ideal point has been identified, which is where the arm's length multiplied by the force's perpendicular component is at its maximum.

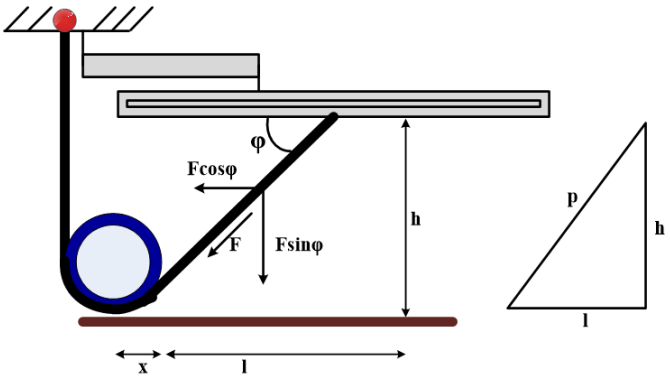

Fig.3.22 Geometry for the determination of position of maximum torque

In the illustration above, *x* represents the distance between the pulley's centre and the arm's hinge, *l* represents the distance from the pulley at which the greatest torque is attained, and *h* represents the vertical distance between the pulley's centre and the setup arm and denotes the angle formed by the shaft's centre and the location of the arm's greatest torque. The motor's distance-exercised torque is given as

$$\tau = F \sin\phi \,.\, (x + l) \tag{19}$$

Figure shows that $\sin\phi = \frac{h}{p}$ where $p = \sqrt{h^2 + l^2}$. Thus, equation (18) can be written as

$$\tau = F.\frac{h}{\sqrt{h^2+l^2}}.(x + l) \tag{20}$$

Equation (20) is a function of 'l', the distance of the maximum torque position from the centre of the shaft as the x, the distance from the centre of the shaft to the hinge of the arm and *h*, the vertical height from the centre of the shaft to the arm are constant.For maximum torque exertion, the derivative of equation (xiii) with respect to l must be equal to zero. Thus,

$$\frac{d\tau}{dl} = 0 \text{ or, } \frac{d}{dl}\left(F.\frac{h}{\sqrt{h^2+l^2}}.(x + l)\right) = 0 \tag{21}$$

The equation can be solved to obtain $l = \frac{h^2}{x}$

Thus the point on the arm where maximum torque is obtained is given by equation (21). The experimental set up has a verical distance of 0.27 metres and the distance betwwen pulley and hinge arm is 0.15 metres. The position of the maximum torque is thereby obtained at a distance of 0.486 metres from the centre of the shaft. Based on the specified condition, a reliable mechanical set up has been developed.

3.4.2.2. Circuitry and controller design

The proposed system is automated and constructed with components that are economical and user friendly. Sensors have been affixed, from which data can be acquired in real time, allowing for the extraction of motor parameters. The motor controller is the most important component of any motor's speed and torque control. In addition to starting and halting a motor, it can serve other purposes. The motor controller circuit varies depending on the application, including on/off toggling circuits, linear control circuits, etc. In this system, a DC motor control circuit that can effectively operate at the system's maximum available load has been designed. Fig.3.23 below depicts the fundamental configuration of the motor driving circuit used in this work.

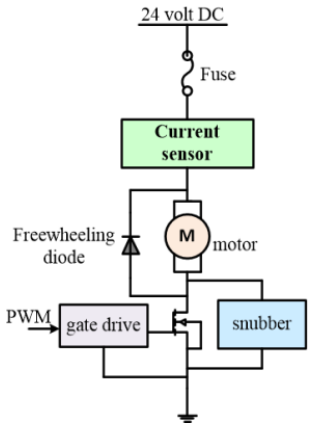

Fig.3.23 Basic configuration of Motor Driving Circuit

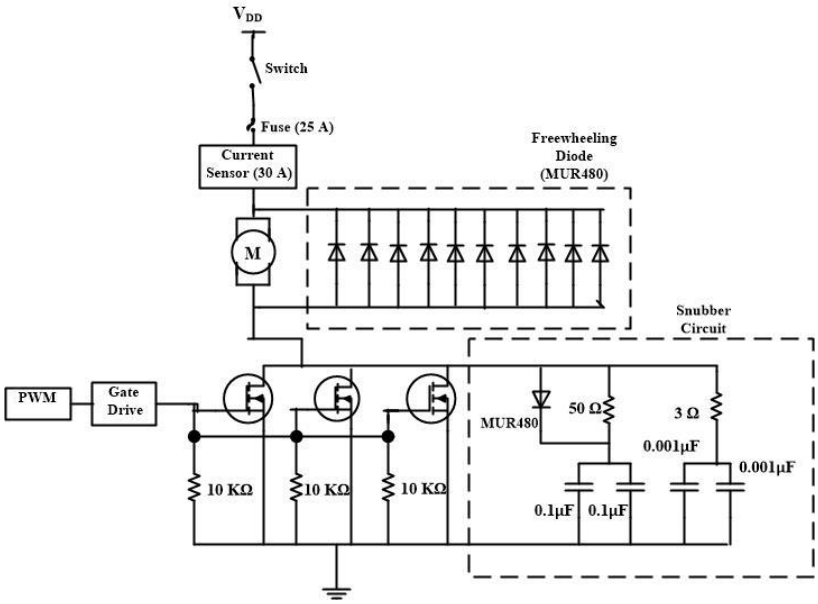

Fig.3.24 Motor Driving Circuit of the System Set-up`

The Motor Controller for the system has been designed to accommodate the motor's maximum allowable current at maximum load. Thus, power MOSFETs are chosen for this application because they can manage more current than BJTs and can also withstand the power electronic losses caused by heat generation. In addition, the $RDS_{(on)}$ value of MOSFET is low and the drive circuit is simple, allowing MOSFET paralleling to be accomplished with simplicity, resulting in less conduction loss. MOSFETs have a temperature coefficient of $RDS_{(on)}$ that is positive, providing thermal stability. To achieve precise and smooth control of the drive motors, a medium PWM frequency range has been used to transition the MOSFETs. Control signals have been implemented using an Arduino AT328P controller. This system employs the IRF3205 Power MOSFET, which has a low $RDS_{(on)}$ value of 8 mΩ and a maximal drain current of 110 A at operating frequency. Parallelly connecting three MOSFETs reduces conduction loss. The voltage overshoots in the presence of the motor, which is an inductive load, and the switching loss of the drive circuit can be reduced by devising an RCD + RC turned off snubber circuit. For controlling the power MOSFET, a gate drive circuit that can convert ON/OFF signals from a controller to power signals is required. The voltage must be applied between the gate and source terminals of the MOSFET in order to generate drain current flow. The purpose of the deliberate gate drive circuit is to parallelly drive three power MOSFETs. In the gate drive circuit, two MCT2E optocouplers with their typical

phototransistor operating modes are connected in a totem pole configuration. It is used to operate the power MOSFET IRF 3205 at 8 kHz. In addition to a turn-off snubber, freewheeling diodes have been added to the circuit. The circuitry involved in the system has been showcased in Fig. 3.24. The system's sensors include a 100 kg load cell, a 30-ampere Hall Effect current sensor (ACS 712) for the detection of current in real time, and an infrared sensor for the calculation of speed. In Table 3.5, the comprehensive list of specifications for the drive and circuit components is tabulated.

Table 3.5 List of major components in the test set-up

Component	**Parameter**	**Peak operating range**	**Purpose**
DC Motor	Current Voltage	100A 25V	Driving wheel
MOSFET IRF3205	Drain voltage Drain current $R_{DS(on)}$ Temperature	55V 110A 8.0mΩ 175°C	DC chopper drive circuit
Opto-isolator	Isolation Rise time Fall time	3.55kV 5µs 5µs	Isolation between control circuit and power circuit
Controller Atmega 328P	Output power Frequency	20mW 16MHz	PWM signal generation
Current Sensor ACS 712	Motor Current Feedback Sensitivity	0-30A at 5V 66mV/A	Current Sensing
Load Cell	Rated Load Excitation voltage	100 kg, 9-12V DC	Calculation of motor load and torque
Battery	Voltage	24V DC	Power supply
Precision Op-amp OP07	Input voltage Supply voltage	$\pm 14\,V$ $\pm 3V \ \pm 18V$	Amplification
Infrared sensor	Working voltage	3.3V to 5V	Speed detection

3.4.2.3. Results and discussion

A DC shunt motor and a PMDC motor have been used to evaluate the experimental setup for extracting motor parameters in real time. Both motors' characteristics have been acquired independently. The DC shunt motor is a 12 Volt, 1200 rpm motor. In contrast, the PMDC motor is a 24 volt, 1 hp motor with a full load current of 39 A and a speed of 3000 rpm. This segment contains results from which various motor-testing parameters are extracted. Motor characteristics and simulation of the motor under various test conditions necessitate the collection of diverse data from the designed configuration. By interfacing Arduino with MATLAB, the different parameters, including input current, input voltage, torque, and speed, are extracted from the setup and the corresponding plots are observed. Calculating the instantaneous power drawn by the motor requires the current and voltage input at various test conditions, whereas the output power delivered by the motor is determined by the product of speed and torque.

a. Results of PMDC motor

The motor characteristics of the PMDC motor were retrieved in real time and are depicted in the figures below. Fig. 3.25 depicts a graph of the motor's real-time speed under no load conditions. Changing the PWM duty cycle or loading the motor can change the speed. It has been discovered that the speed is accurately plotted with regard to time. Fig. 3.26 shows a real-time graph of torque delivered to the motor at various testing intervals. The torque is provided mechanically by breaking the belt fastened over the pulley linked to the motor shaft. Fig. 3.27 depicts a graph of the real-time current drawn by the motor during the test interval. The current flowing through the motor increases as the PWM duty cycle or applied load increases. Because of the fundamental DC motor characteristics, the motor starting current increases as soon as the motor begins to accelerate. As shown in Fig. 3.28, the input and output power can be compared in real time. It can be observed that the efficiency is less than one, and that the efficiency fluctuates depending on the load conditions. As a result, the most efficient operational point can be determined.

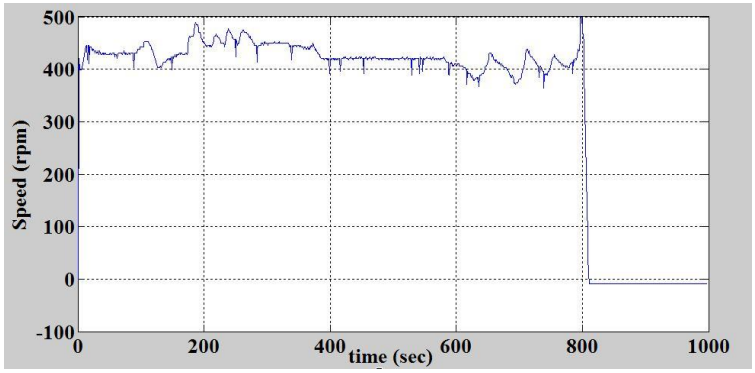

Fig.3.25 Real-time data extraction of speed with time

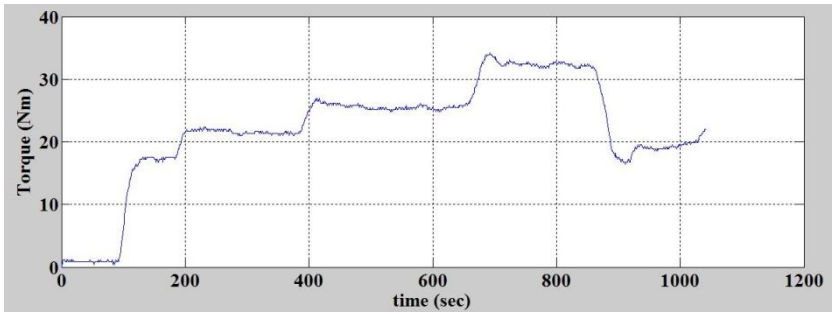

Fig.3.26 Real-time data extraction of torque with time

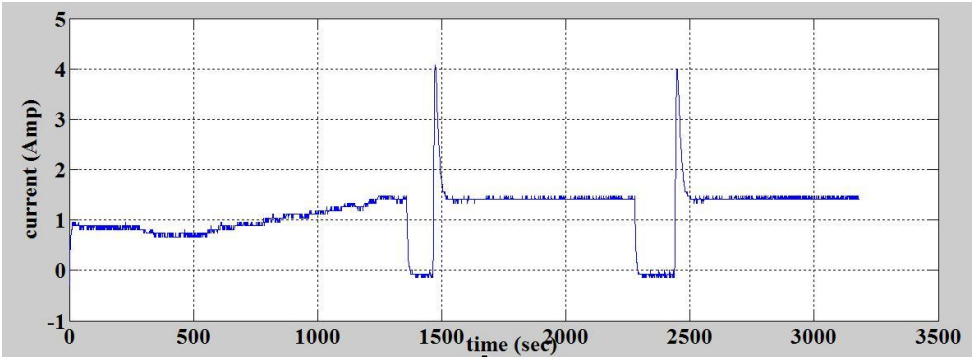

Fig.3.27 Real-time data extraction of motor current as a function of time

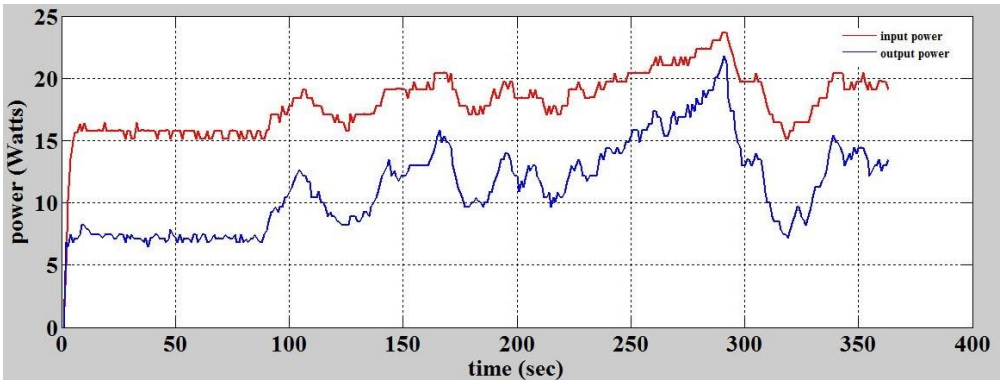

Fig.3.28 Real-time data extraction of power through the motor as a function of time

b. Results of DC Shunt Motor

Figures 3.29 to 3.32 depict the extracted plots for various motor parameters of the DC Shunt motor. The motor speed is dependent on the input voltage. The graph in Fig.3.29 illustrates the change in motor speed over time. The utmost speed of the motor with no load is 1200 RPM at a DC input voltage of 12V. Minimum average voltage of 3V is required to restart the motor after it has stalled. Fig.3.30 depicts the variation in motor speed with PWM input when the motor is under a 1.4 Nm strain. The above plot demonstrates that when the load is applied at zero RPM, the required voltage to initiate the motor from stall is greater than in the absence of load.

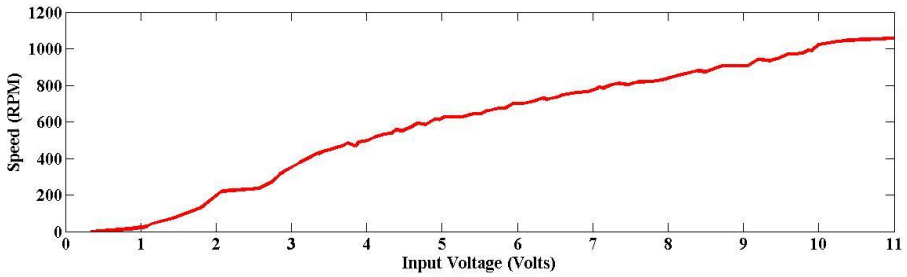

Fig.3.29 Variation of motor speed with respect to Input Voltage at no load

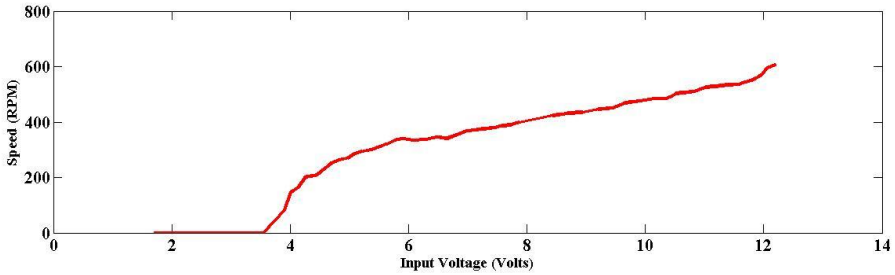

Fig.3.30 Variation of motor speed with respect to Input Voltage at 1.4 Nm load

Figure 3.31 illustrates the correlation between the speed and input voltage of the shunt DC motor when subjected to a 6 Nm load. The initial voltage supplied to the motor is estimated to be around 5 volts. When the input voltage is incrementally raised from 0 to 12 Volts, the motor initiates motion from a stationary state when exposed to a greater load accompanied by an elevated input voltage. The power output of the motor is determined by the product of its torque and angular velocity. The motor's output power is determined by the product of torque and speed, as there exists a trade-off between these two parameters and the output power must be lower than the input power. The velocity of the motor exhibits a negative correlation with the magnitude of

the load. Figure 3.32 depicts the correlation between torque and motor speed under a 50% duty cycle.

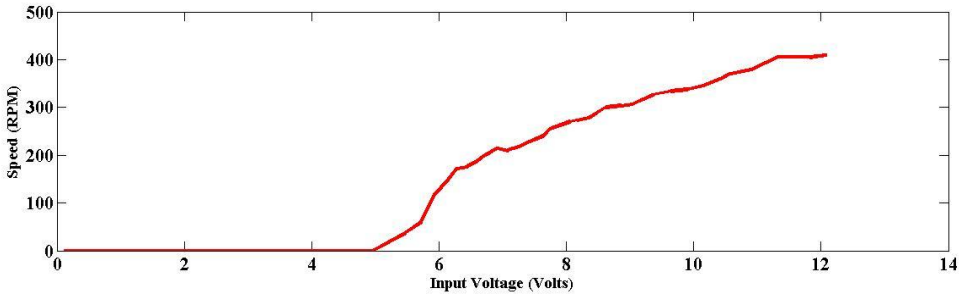

Fig.3.31 Variation of motor speed with respect to Input Voltage at 6 Nm load

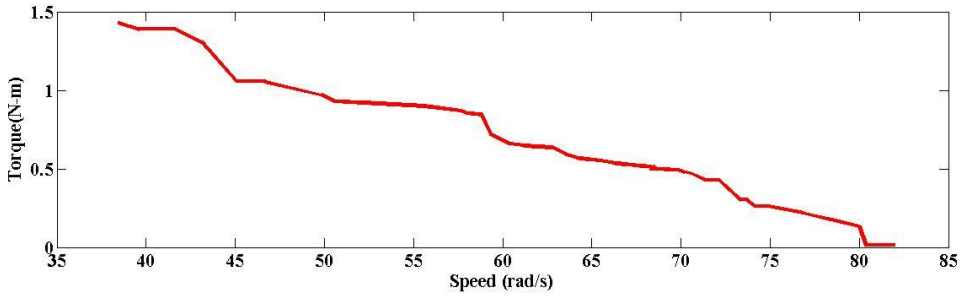

Fig.3.32 Real time Speed-Torque Graph at 50% Duty Cycle

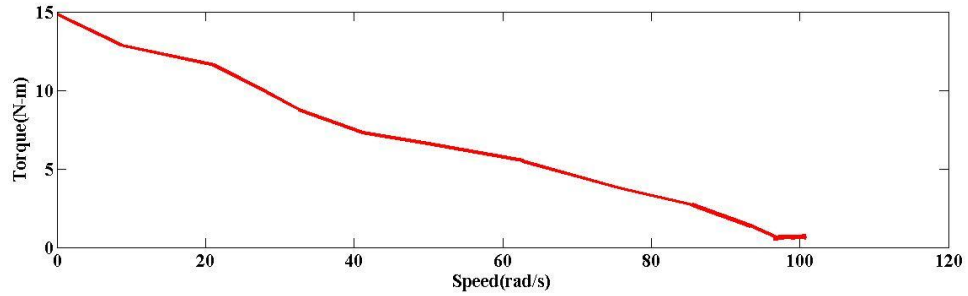

Fig.3.33 Real time Speed-Torque Graph at 100% Duty Cycle

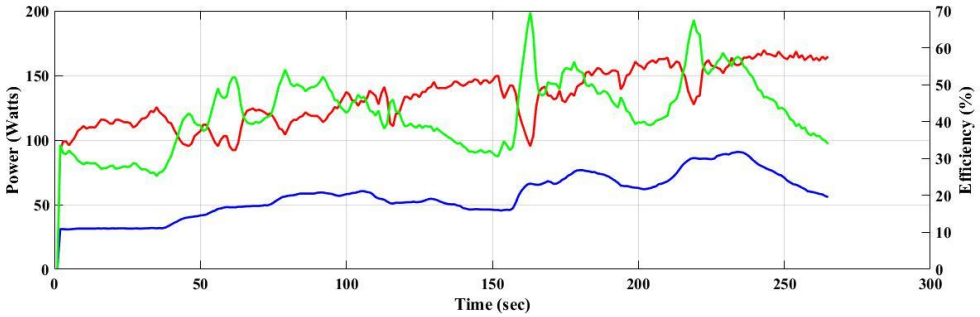

Fig.3.34 Real time graph of input power, output power and efficiency with time

The torque-speed relationship of the motor at 100% duty cycle is depicted in the graph above in Fig. 3.33. The output torque is at its peak when the speed is close to a halt, and it decreases as the speed increases. At various duty cycles, the speed-torque curve displays the same pattern. The output power of the motor is a function of the torque and the angular velocity at any operating voltage. Using the input and output power, the efficiency can be extracted dynamically at any given load. When the load associated with the motor changes, the input current subsequently increases, as does the input power. Consequently, the torque of the motor increases, and so does the output power. The motor shows variation in efficiency at dynamic loading conditions. In Fig.34, the red, blue, and green lines represent the input power, output power, and efficiency of the DC shunt motor, respectively. Different sections of the graphs depict the input, output, and efficiency at various loads. The y-coordinates on the left of the diagram indicate the input and output power in watts, while the y-coordinates on the right indicate the efficiency in percentage. When a load is applied to a motor, the input current and input power both increase. Consequently, both the torque and output power of the motor increase. The motor's efficacy varies under various load conditions. Consequently, the optimal operational point can be derived from the above graph. Using the test configuration for the DC shunt motor, it can be concluded that the motor operates most efficiently when its load is just below its maximum rated torque. When the input power is approximately 98 Watts, the output power is seen to be approximately 67 Watts. The efficiency is therefore calculated to be around 70%. Hence, the most efficient operating point can be automatically determined from the generated curves.

Results show that motor parameters were extracted and displayed under all dynamic loading conditions using the Arduino-MATLAB interface. The developed system includes inexpensive sensors, actuators, and power drive circuits. The output of the system as a whole is deemed reliable and adequate to match the theoretically predicted results. Nonetheless, a few trivial commutation and interfacing noises appeared to have a minor impact on the actual nature of the system-generated curve. This could be remedied by isolating the system effectively and averting other electromagnetic interferences. Using a high-speed microcontroller and costly, highly stable sensors could improve the performance of a system intended for use on a high-speed dynamic test platform.

3.4.3. Extraction of motor parameters with electronic load

An eco-routing system assists in determining the most energy-efficient route between the source and the destination when travelling between two known sites. However, this approach is based on a variety of criteria, and many researchers are working to identify the most important factors responsible for efficient identification. The load experienced by the motor during the trip, and hence the efficiency with which it operates, is directly linked to the vehicle's energy consumption. Minimisation of energy consumption is the primary goal of eco-routing; therefore, detecting numerous aspects related to the motor as well as its features can be extremely beneficial in developing an energy-efficient system. The prior method employed a mechanical load in the procedure, which, while theoretically easy, required more effort on the part of the user for the application of bigger loads. The system was pulley and belt driven, with an unaccounted for friction loss. It also necessitated the use of additional measuring equipment, such as a spring balance or torque metre. As a result, another system has been built to address those concerns in order to make the procedure simpler and more user-pleasing. The system is based on motor-generator coupling technology, which employs an electronic load to get various DC motor properties. Because the weight is applied electronically, mechanical assistance is substantially minimised here. Electrical loads have minimal advantages over mechanical loads. Because there is no loss due to friction, the accuracy of these loads is higher than their mechanical counterparts. It also minimises the system's overall weight and flexibility. Electrical loads can be changed in a large range, whereas mechanical loads are limited by the setup. Attempts have been made to make the configuration as easy and efficient as feasible. The test setup was built with commercially available electronic components and interfacing tools. Because the system outputs are obtained in real time, they can be used onboard electric vehicle test systems without any difficulty.

3.4.3.1. System design

The method presented in this study utilises a motor-generator coupling mechanism to retrieve motor characteristics at varying voltages. A motor generator (M-G) set is a composite apparatus comprising a motor and a

generator that are mechanically interconnected by a common shaft. Motor generator sets are commonly employed for the purpose of transforming the voltage, phase, and frequency of electrical power. For the connection to be functional, it is imperative that the rated speeds of both the motor and the generator are identical. In the conducted experiment, two Permanent Magnet Direct Current (PMDC) motors, with identical specifications, were employed. The motor-generator linked set is formed by joining them end to end with a single shaft. The motor is externally powered by a 24V lead acid battery supply, which in turn causes the rotation of the generator's rotor. The supply line serves as the conduit for delivering electrical energy to the motor. The rotation of the shaft causes the generator to also receive mechanical input due to its mechanical association with the shaft. Consequently, the generator is capable of producing electrical output power, thereby facilitating the conversion of mechanical energy into electrical energy. The power sent between the machines is in the form of mechanical torque, despite the fact that both the input and output sides operate on electrical power. This configuration facilitates the isolation of the electrical system and also incorporates a power buffering mechanism between the two electrical systems. The block diagram of the total system configuration is illustrated in Figure 3.35. Two 24-volt, 350-watt PMDC motors power the system. The armature voltage control method uses pulse width modulation (PWM) technology to control the motor speed. A potentiometer is used in this technique to control the speed by varying the duty cycles. As illustrated in Fig. 3.35, two different ammeters are connected in the circuit for real-time measurement of the armature current under varied loading circumstances. It also features two voltmeters for measuring both the input and output voltages. A non-contact tachometer is used to measure the speed of the motors. A drive circuit with input from a microcontroller powers the motor. The generator rotates at the same rate that the motor is powered. As a result, energy is transferred from the motor to the generator. The input is fixed at a specified duty-cycle during the experiment, so a steady current is drawn from the battery supply. After the input power is fixed, the generator portion of the circuit is loaded. A separate power circuit is attached to the generator and is controlled by a separate microprocessor. The load is made up of 24 V DC resistive bulbs. The potentiometer is then

gradually increased, which increases the load, allowing more current to be drawn and producing power outputs at varied load values. The current and voltage flowing through the motor-generator set are monitored in real time.

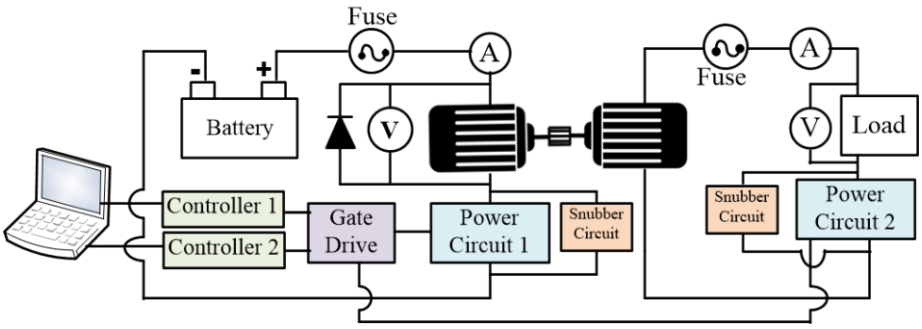

Fig.3.35 Block diagram of the proposed system

Fig.3.36 The experimental set-up used for estimation of DC motor characteristics

Table 3. 6 Components used in the experimental set-up

Item No.	Component
1	24V DC Battery
2	Motor
3	Motor acting as the generator
4	Common shaft
5	Power circuit and snubber
6	Load (Resistive bulb)
7	Current sensor
8	Potentiometer

3.4.3.2.Circuitry and data acquisition

An armature voltage controlled PWM technique is used to power the motor, which uses a dedicated switching circuit. In Fig. 3.36, the experimental setup has been depicted, the components of which are specified in Table 3.6, and indicated by numbers. Two distinct power circuits connected to the motor

and generator allow for independent control of each. Since they are connected by a common shaft, the generator runs at the same speed as the motor, but when a load is supplied to the circuit, its own power circuit is employed. Because of their fast switching times and low power dissipation, power MOSFETs were used in the design of the power circuit. To handle the motor's large starting and running current needs while lowering the circuit's on-state resistance and conduction loss, a DC chopper circuit with a total of 6 MOSFETs connected in parallel has been designed. To provide accurate and spherical drive motor control, the power MOSFETs are switched at an 8 kHz frequency. The requisite PMDC motors' effective speed control has been maintained by utilising the necessary gate drive and snubber circuits. The power signals have been created by converting the ON/OFF signals from a controller using a gate driver. For the current to flow through the drain of the MOSFET, voltage must be provided between the gate and source terminals. Prior to developing the circuit, the appropriate estimations for the drive circuit's conduction loss and switching loss were made. Each MOSFET's gate and source are each coupled to a 10 kHz pull-down resistor to lessen gate charge. Because it is crucial for switching the MOSFETs, a turn off RC snubber circuit has also been incorporated into the driving circuit. This system does not utilise a turn-on snubber circuit since the inductive load limits the initial current. The turn-off snubber has been employed to stop erratic current distribution, which could lead to switch overheating and damage. If there is a significant surge at the time of switching, it offers an alternative path for the current flow. The voltage characteristics of the load were used to estimate the values of the various components in the snubber design. The specifications of various circuit components used in the suggested system are listed in Table 3.7. Sensors and microcontrollers are used to interface with the various motor characteristics. Fig. 3.37 illustrates the circuitry and the interface module of the system in a block diagram. The designed snubber circuit has also been shown in that diagram. Real-time monitoring of the current and voltage of the motor-generator set is done. The use of electrical loads has also streamlined the interfacing process, as they can be acquired directly without requiring the use of a separate system to transform mechanical data into a graphical user interface.

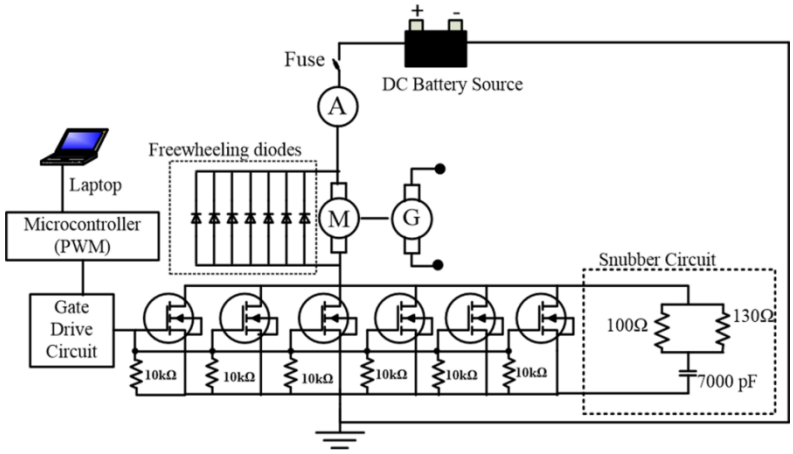

Fig.3.37 Illustration of circuitry used in the proposed set-up

Table 3. 7 Technical specifications of components used in the experimental set-up

Component	**Parameter**	**Op. range**	**Purpose**
PMDC Motor	Power Voltage	350 W 24V	Driving motor
MOSFET IRF3205	Drain voltage Drain current	55V 110A	DC chopper drive circuit
Controller Atmega 328P	Output power Frequency	20mW 16MHz	PWM signal generation
Current Sensor ACS 712	Current feedback Sensitivity	0-30A at 5V 66mV/A	Current Sensing

3.4.3.3. Calculations involved

The effectiveness of electric motors as an evaluation criterion has gained importance in combination with continuous attempts for energy minimization in all worldwide arenas, particularly the electric car sector. About 70% of industrial power usage is accounted for by electric motor driven systems [29]. Efficiency is therefore a key quality. It has previously been stated that the nominal efficiency alone is insufficient to accurately assess an electric motor's energy usage in actual use [30]. Motor efficiency tends to rapidly decline below 50% due to a range of mechanical and electrical flaws within the motor. The ratio of the input power to the output power, as specified in equation (22), is what is known as a DC motor efficiency.

$$\eta_{\text{motor}} = \frac{\text{Mechanical Power Output}}{\text{Electrical Power Input}} \times 100\% \qquad (22)$$

The input power is the power that goes into the armature and is given by equation(23) as

$$\text{Input Power} = VI_a \tag{23}$$

Where, V is the applied voltage in volts and I_a is the current through the armature measured in Amperes. The output power (P_{out}) on the mechanical side is the product of the torque generated (in Newton metres) and the angular speed(ω),whose value can be determined from equation(24).

$$P_{out} = T.\omega \tag{24}$$

Here, Tis the torque and ω is the angular speed in rad/sec. rpm represents the rotations per minute and is expressed as

$$\omega = \frac{2\pi}{60}.\text{rpm} \tag{25}$$

The torque of a motor is subject to variation in relation to its speed. In the absence of a load, torque is absent when the system is operating at its maximum speed. The application of a load results in an increase in mechanical resistance. To surmount this resistance, the motor initiates an increase in current consumption, resulting in a subsequent decrease in speed. The cessation of motor operation occurs when the load is augmented to a specific magnitude, commonly referred to as stall torque. Analysis of the torque speed characteristics can be employed to ascertain the stall torque.

3.4.3.4.Results and discussion

The proposed system has been utilised to ascertain the prime parameters of the PMDC motors used in the test electric vehicle. This procedure helps in the analysis of the motor's optimal and most efficient operating range. The use of electronic elements in this method permits the collection of a wide variety of data. This method has yielded data on parameters such as speed, torque, current, voltage, and efficiency.

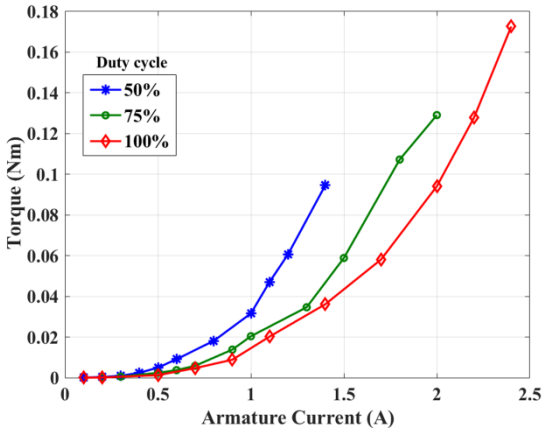

Fig.3.38 The torque versus armature current characteristic of the PMDC motor

Fig. 3.38 depicts the torque versus armature current curve, often known as the electrical characteristic, at various duty cycles. The torque is proportional to the armature current multiplied by the field flux. In the case of PMDC motors, however, the field flux is believed to be constant and can be ignored. This is clearly visible in the curve, where an increase in armature current leads to an increase in motor torque. It can be seen that as the load grows, so does the motor's current consumption, resulting in a drop in motor speed.

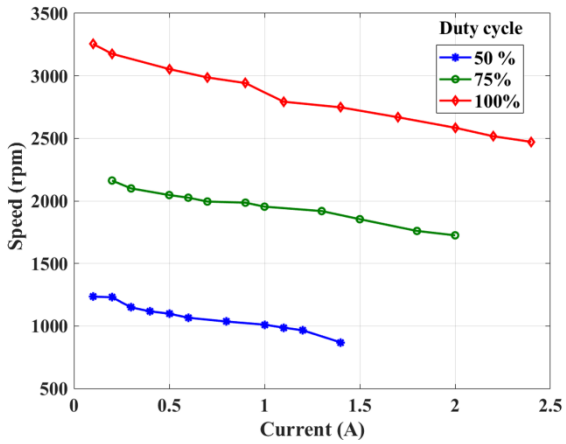

Fig.3.39 The speed versus current characteristic of the PMDC motor

Fig. 3.39 depicts the characteristics of speed versus current for various input voltages. When the load current is modest, the change in back emf is negligible. Since flux is presumed to be constant in PMDC motors, speed can be considered proportional to the back emf. If the back emf remains

unaltered, the speed should remain unchanged in ideal circumstances. However, the above curve demonstrates that under practical conditions, both flux and reverses emf decrease with load. The decrease in back emf is marginally greater than the decrease in flux, resulting in a slight decrease in velocity. Typically, the speed decreases by only 5 to 15% of the speed at maximum load. The torque-speed characteristic curve at various duty cycles is depicted in Fig. 3.40. This curve is also known as the curve of mechanical characteristics. Torque and velocity can be observed to be inversely proportional.

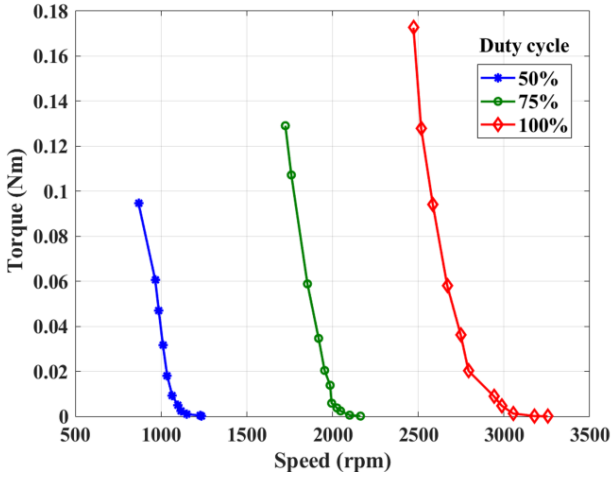

Fig.3.40 The torque versus speed characteristic of the PMDC motor

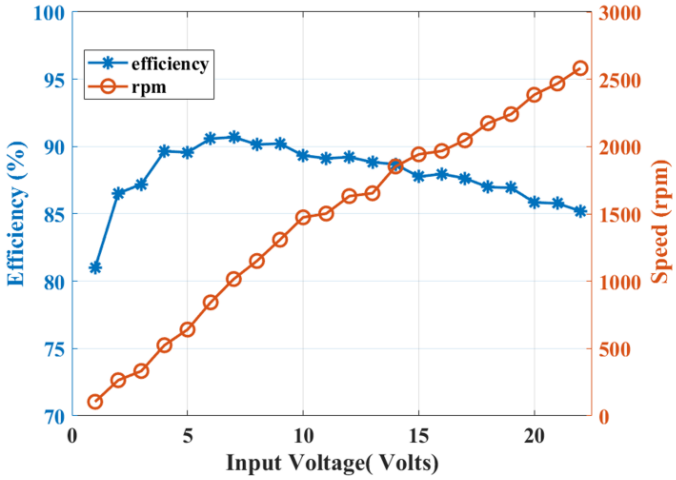

Fig.3.41 The efficiency of the motor at various voltages along its line of operation

The input and output power can be accurately approximated based on the system configuration. The circuit's power loss can also be readily calculated. The estimated loss demonstrates the motor's efficiency. Fig. 3.41 depicts

such a condition when no load is attached to the system. It depicts the efficacy of the motor at various input operating voltages as well as the speed along the operating line. The curve shows that the motor can achieve efficiency as high as 85–90% and reach a maximum rpm of 2700. The above results were derived from experimental data and demonstrate that the proposed system can be used to extract motor parameters with relative ease. Based on a motor-generator conjunction technique, a straightforward and semi-automated system for extracting motor parameters has been created. The circuitry is effective in determining the properties and is reasonably priced. The use of an electronic load rather than a mechanical load enables testing under dynamic loading situations, reduces system losses, and increases system flexibility. The best operating range for PMDC motors when employed in the test EV has been determined through experimentation. Results resemble properties listed in datasheets for commercial products. The use of speed sensors can improve the automation of this system. It may be concluded that this method removes the difficulties associated with using a mechanical load and makes it possible to use it in sophisticated motor control applications.

3.5. Conclusion

This chapter summarises electric vehicle design and development. It emphasises the importance of vehicle dynamics when designing a vehicle. A test electric vehicle prototype required for the implementation of an eco-routing navigation system has been designed and developed. It is a neighbourhood battery electric vehicle and weighs around 120 kg. It is independent rear-wheel driven and has PMDC motors attached to it for propulsion. To attain the main aim of calculating the energy consumption of an EV, different sensors have been installed in the EV. Test runs have been successfully performed on the EV. Electric motors are the prime mover of industry and our general comfort in commercial buildings. Output power and efficiency are major parameters that need to be analysed when electric motors are being used, especially for electric vehicles. The characterisation of the motors used is equally important, and therefore a technique to determine the motor characteristics has been proposed. A universal motor parameter extraction system has been designed

and developed for the extraction of various parameters of DC motors. The system has been tested with a 1 hp PMDC motor and a DC shunt motor. Validated results were extracted and accurately displayed using MATLAB interfacing under any dynamic loading conditions, and the same has been compared with the value observed by using the corresponding measuring instrument. It has been compared and seen that an error of 1.13% in speed characteristics, 0.13% in torque characteristics, and approximately 2% in efficiency exists. The developed system incorporates low-cost sensors, actuators, and simple power drive circuits. The output of the overall system is found to be reliable and sufficient to match the expected theoretically calculated results. In addition, a simple and semi-automated system for the extraction of motor parameters based on a motor-generator coupling technique has been designed and developed. The circuitry used is cost-efficient and proves efficient in the determination of the characteristics. The utilisation of an electronic load, as opposed to a mechanical load, enables the examination of dynamic loading circumstances, facilitates the mitigation of losses within the system, and enhances the system's overall flexibility. Experimentation has been performed on PMDC motors to determine their optimal working range when used in the test EV. Results resemble characteristics available in commercial datasheets. Future works involve full automation of the system, where speed sensors can be used to obtain real-time data. The system can also be designed to test and characterise AC motors. It can be concluded that this technique eliminates the hurdles faced when a mechanical load is being used and opens avenues for its use in advanced motor control.

References

[1] *Ministry of Heavy Industries. FAME India* .Retrieved on 10 Sep.2021 from https://pib.gov.in/PressReleasePage.aspx?PRID=1577880, 09 July, 2019.

[2] *EV design – introduction*. Retrieved on 06 Jul. 2022 from https://x-engineer.org/ev-design-introduction/

[3] Situ, L. Electric vehicle development: the past, present & future. In *3rd International Conference on Power Electronics Systems and Applications (PESA)*, pages 1-3, IEEE, May 2009.

[4] *Vehicle dynamics.* Retrieved on 16 Oct. 2021 from https://en.wikipedia.org/wiki/Vehicle_dynamics#:~:text=For%20motorized%20vehicles%2C%20such%20as,surface%2Fwater%20conditions%2C%20etc .

[5] Jazar, R.N. *Vehicle Dynamics: Theory and Applications*, 2008 Springer Science+ Business Media, 2008.

[6] *OxTS Reference Frames and ISO8855 Reference Frames.*Tetrieved on 23 Jan.2022 from https://support.oxts.com/hc/en-us/articles/115002859149-OxTS-Reference-Frames-and-ISO8855ReferenceFrames#:~:text=ISO%208855%20vehicle%20system%3A&text=of%20the%20vehicle.-,The%20X%20axis%20is%20parallel%20to%20the%20vehicle's%20heading%20and,up%20direction%20of%20the%20vehicle.

[7] *Neighbourhood electric vehicles*. Retrieved on 05 Apr. 2023 from https://www .gemcar.com/ neighborhood-electric-vehicles/.

[8] *Difference between Chain Drive and Belt Drive*. Retrieved on 24 May.2022 from https://www.tutorialspoint.com/difference-between-chain-drive-and-belt-drive.

[9] *Why choose a belt drive over a chain drive?*. Retrieved on 25 May.2022 from https://www.acorn-ind.co.uk/power-transmission/industrial-belts/details/#:~:text=Lower%20maintenance20requirements,to%20environmental%20contamination%20than%20chain.

[10] *Introduction to Load Cells.* Retrieved on 23 Aug. 2022 from *https://in.omega.com /prodinfo/loadcells.html.*

[11] *Load cell working principle.* Retrieved on 23 Aug. 2022 from https://instrumentationtools.com/load-cell-working-principle/.

[12] *Rotary Encoder Arduino Code Detail Guide.* Retrieved on 12 Oct.2021 from https://robu.in/run-rotary-encoder-arduino-code/, 17 January, 2017.

[13] *Hall Effect Sensor*. Retrieved on 16 Feb. 2022 from https://en.wikipedia .org/wiki/ Hall_effect_sensor.

[14] *Fully Integrated, Hall-Effect-Based Linear Current Sensor IC with 2.1 kV$_{RMS}$ Isolation and a Low-Resistance Current Conductor*. Retrieved on 16 Feb.2022 from https://datasheetspdf.com/pdf-file/570845/AllegroMicro Systems /ACS712/1.

[15] *ACS712 Current Sensor Working and Applications.* Retrieved on 16 Feb.2022 from https://www.elprocus.com/acs712-current-sensor-working-and-applications/.

[16] Pedley,M. *Tilt Sensing Using a Three-Axis Accelerometer*.Freescale semiconductor, Document Number: AN3461 Application Note,Rev. 6, March 2013.

[17] *MPU-6000 and MPU-6050 Product Specification Revision 3.4* . Retrieved on 14 Feb.2022 from https://datasheetspdf.com/pdf-file/735134/InvenSense/MPU6050/1.

[18] Smith, G.M. *Data Acquisition (DAQ)-The ultimate guide.* Retrieved on 15 Sep. 2022 from https://dewesoft.com/blog/what-is-data-acquisition, 28 June, 2022.

[19] *Determining electric motor load and efficiency*. Retrieved on 09 Dec.2019 from http://energy.gov/eere/amo/downloads/determining-electricmotor-load-and-efficiency.

[20] Sweeting, W.J., Hutchinson, A.R. and Savage, S.D. Factors affecting electric vehicle energy consumption. *International Journal of Sustainable Engineering*, 4(3):192-201, 2011.

[21] Saab, S.S. and Kaed-Bey, R.A. Parameter identification of a DC motor: an experimental approach. *In ICECS 2001, 8th IEEE International Conference on Electronics, Circuits and Systems*, volume 2, pages 981-984, Malta , 2001, doi: 10.1109/ICECS. 2001.957638.

[22] Rubaai, A. and Kotaru, R. Online identification and control of a DC motor using learning adaptation of neural networks. *IEEE Transactions on Industry Applications*.36 (3):935-942, May-June 2000, doi: 10.1109/28.845075 .

[23] Narendra, K.S. and Parthasarathy, K. Identification and control of dynamical systems using neural networks. *IEEE Transactions on Neural Networks*,1(1): 4-27, 1990.

[24] Huynh,D.C. and Dunnigan, M.W.Parameter estimation of an induction machine using advanced particle swarm optimization algorithms.*IET*.4(9):748–760, 2010.

[25] Torque Equation of DC Motor. Retrieved on 02 Dec. 2019 from https://www.electrical4u.com/torque-equation-of-dc-motor/.

[26] *DC Shunt Motor: Speed Control, Characteristics & Theory*. Retrieved on 07 Apr. 2023 from https://www.electrical4u.com/shunt-wound-dc-motor-dc-shunt-motor/ , 25 October 2020.

[27] Circuit globe. *Permanent magnet DC motor*. Retrieved on 05 Apr. 2023 from https://circuitglobe.com/permanent-magnet-dc-motor.html.

[28] Larminie, J. and Lowry, J. *Electric vehicle technology explained*, John Wiley & Sons, 2012.

[29] De Keulenaer, H. Energy efficient motor driven systems. *Energy & Environment*,15(5):873-905, 2004, doi:10.1260/0958305042886688.

[30] Auinger, H. Efficiency of electric motors under practical conditions. *Power Engineering Journal*, 15 (3):163-167 , 2001, doi: 10.1049/pe: 20010309.